Supplementary Information for:

The evolution of red color vision is linked to coordinated rhodopsin tuning in lycaenid butterflies

Marjorie A. Liénard, Gary D. Bernard, Andrew Allen, Jean-Marc Lassance, Siliang Song, Richard Rabideau Childers, Nanfang Yu, Dajia Ye, Adriana Stephenson, Wendy A. Valencia-Montoya, Shayla Salzman, Melissa R.L. Whitaker, Michael Calonje, Feng Zhang, Naomi E. Pierce

Corresponding authors: Marjorie A. Liénard, Naomi E. Pierce

Email: marjorie.lienard@biol.lu.se, npierce@oeb.harvard.edu

This PDF file includes:

Supplementary Methods

Supplementary References

Supplementary Figures 1 to 10

Supplementary Methods

Epi-Microspectrophotometry

Three epi-microspectrophotometry (MSP) experimental methods are used to study the properties of the multiple rhodopsins of a butterfly ommatidium: *in vivo* photochemistry, retinal densitometry, and optophysiology (see below for details). Rhodopsins are packaged within a long, thin rhabdom waveguide that is illuminated efficiently by cornea and cone at one end (13) and terminated optically by a tracheolar tapetum at the basal end (16) (Fig. S4A). Light propagates down the rhabdom waveguide, being partially absorbed by the multiple rhodopsins and metarhodopsins as it goes. Light that survives the inward trip, and is reflected by the tapetum, propagates back up the rhabdom, again being partially absorbed. Light that survives this double pass through the rhabdom is collected by the cone and cornea, then passes out of the eye where it is observable as a narrow beam of eyeshine. Thus, the time-dependent reflectance spectrum of ommatidial eyeshine contains information about absorbance spectra of rhodopsins and metarhodopsins, reflection spectrum of the tapetum, and photoreceptor physiological responses. Eyeshine spectra also depend upon both the history of illumination and the duration of dark-time preceding measurement of an eyeshine spectrum, because the metarhodopsin content of the rhabdom decays exponentially with time in the dark, as rhodopsin content recovers at a slower rate than metarhodopsin decays.

Eyeshine measurements used for photochemical analyses from butterfly eyes follow procedures described previously (9, 18-20). Accordingly, a completely intact butterfly was mounted in a slotted plastic tube fixed to a goniometric stage and oriented to select a particular eye region for study. Then the microscope objective was focused inward to collapse all eyeshine into a small central spot. The field stop is adjusted to mask that spot and exclude the scattered light surrounding it. After at least two hours in the dark in warm surroundings, a reflectance spectrum is measured with a series of dim monochromatic flashes. This is used as a dark-adapted reference spectrum against which difference spectra are computed following treatment with photo-isomerizing flashes.

All long-wavelength (LW) rhodopsins shift peak absorbance to shorter wavelength upon photo-isomerization. Thus, a strategy for characterizing the spectral properties of the rhodopsin most sensitive at long wavelengths is to flash the eye using each of a graded series of sharp-cutoff, long-pass color filters, working from long-wavelength cutoff to short, measuring a reflectance spectrum after each delivery. This procedure is halted when a flash causes a measurable difference spectrum. A partial bleach is created by changing to the next filter in the series and delivering repeated flashes then monitoring dark-recovery by occasionally measuring reflectance spectra and determining the metarhodopsin decay rate. When the amount of metarhodopsin is no longer measurable, rhodopsin has not yet recovered fully, so the difference spectrum, at that time, is a direct measure of the rhodopsin absorbance spectrum. An estimate of that spectrum and its λ_{max} is obtained by non-linear least-squares fitting to Bernard's polynomial template (4).

In vivo Photochemistry. When rhodopsin is photo-isomerized to become metarhodopsin, it undergoes a spectral shift in the absorbance spectrum. For LW rhodopsins, the shift is to shorter wavelengths (hypsochromic); the metarhodopsin peak is usually between 490 nm and 500 nm. For both UV-absorbing and blue-absorbing rhodopsins, the shift is to longer wavelengths (bathochromic), typically to 475 nm - 490 nm. These photochemical changes are observable in eyeshine reflectance spectra, as increased reflectance caused by loss of rhodopsin, and decreased reflectance caused by the metarhodopsin. The computed absorbance-difference spectrum (DS), therefore, has a positive peak caused by accumulation of metarhodopsin (M), and a negative peak caused by loss of rhodopsin (R) (Fig. 2).

The absorbance difference spectrum relaxes with time in the dark, but changes shape in doing so; the positive peak relaxes to zero much faster than the negative peak. The entire temporal evolution of difference spectra can be reproduced quantitatively by assuming different kinetics for the dark-processes of metarhodopsin decay and rhodopsin recovery. Metarhodopsin decay is well approximated by a single exponential process, but the metarhodopsin decay time constant is a strong function of temperature. Rhodopsin recovery is considerably slower than metarhodopsin decay, making it possible to create a partial bleach using repeated episodes of bright flashes followed by dark periods during which metarhodopsin decays totally from the rhabdom. The difference spectrum for that partial bleach is a direct measurement of the absorbance spectrum of the LW rhodopsin (19). Similar experiments with photoconversion of the other spectral types of rhodopsin are more complicated because a bright blue flash designed to efficiently photo-isomerize blue-absorbing rhodopsins will also convert some LW rhodopsins to their metarhodopsins, although with less efficiency. However, if the LW rhodopsins are first bleached, then difference spectra for the blue rhodopsin are measurable. Accordingly, before photoconversion of the *E. atala* blue rhodopsin (Fig. S2A), the LW rhodopsins were partially bleached by flashing with exposure to RG645 (20s, 2s ON /55s OFF). After resting in the dark for 24 min for metarhodopsins to decay, the eye (Elevation 0° and Azimuth 10°) was flashed with 12s RG430 (2s/60s), which converted blue rhodopsin to its metarhodopsin M505. A difference spectrum for R440 was computed from reflectance spectra measured before and 9 min after the series of bright blue flashes.

Optophysiology. Photoreceptor cells in butterfly eyes contain intracellular pigment granules that move centripetally in response to bright illumination and deplete light from the rhabdom by scattering and absorption. This process creates an effective pupillary response observable as a decrease in eyeshine reflectance (24). This intracellular pigment migration is mediated exclusively by photo-isomerization of the rhodopsin contained within the same cell's rhabdomere and is not influenced by physiological responses of neighboring ommatidia. Thus, the pupillary pigment granules can be used as an optically measured intracellular probe of physiological responses to light from that cell (25).

A double-beam epi-MSP apparatus was used for optophysiological measurements of pupillary sensitivity. One beam is deep-red filtered (e.g., 710 nm), and used to monitor continuously the reflectance of eyeshine but does not itself cause a pupillary response. The second beam delivers a monochromatic flash that evokes a pupillary response, measured by the first beam as a decrease in deep-red eyeshine reflectance. At each stimulating wavelength, the flash intensity is adjusted with computer-controlled neutral-density wheels to produce a criterion decrease in reflectance (usually 3% to 5%). The wavelength sequence is randomized, and both flash duration and inter-stimulus interval are held constant. After completing an experimental series, the butterfly is replaced by a factory calibrated Hamamatsu S1226 photodiode and quantum flux Q measured for every criterion combination of wavelength and wheel setting. Spectral sensitivity is computed as $S(\lambda) = 1 / Q(\lambda)$.

Retinal densitometry. The visual pigment content of rhabdoms can be estimated quantitatively when the tapetal reflectance spectrum is constant (white) for wavelengths shorter than about 600 nm (9, 20). A computational model based on an electron micrograph of the tracheolar tapetum shows that this "chirped" set of layers functions as a broadband reflecting interference filter exhibiting a computed reflectance greater than 90% for wavelengths between 320 and 680 nm, thereby justifying the assumption of a white reflectance spectrum in that band. This property of wideband white tapetal reflectance can be exploited to computationally estimate rhodopsin contents. It is most valuable when applied after λ_{max} of UV, blue, and LW rhodopsins have been determined from *in vivo* photochemistry and optophysiology.

The procedure to quantify R362, R441, and R564 in *E. atala* was sequential. First, a reflectance spectrum was measured after all metarhodopsins had decayed from the rhabdoms, e.g., after overnight adaptation of the eye in the dark (black-filled circles). Next, the dark spectrum was stripped of round-trip optical density (OD) 1.50 of R564 rhodopsin so that the residual spectra (red lines) were flat from 570 nm out to the 690 nm roll-off of tapetal reflectance (Fig. S2). Next, those residual spectra were stripped of OD 0.42 of R441 (cyan lines), leaving large dips in the blue-green around 500 nm that were poorly fit by a single blue opsin. However, stripping of OD 0.82 λ_{max} 395 (Retinal Binding Protein, RBP) left UV residues (magenta lines) well fit by density of 0.35 of R362. The remaining residuals (blue lines) were subjected to least-squares fitting to the rhodopsin template, which produced excellent R494 fits of 0.76 supporting the presence of the fourth rhodopsin, R494. Optical densities for female *E. atala* rhodopsins, determined following the same procedure are 1.00 (R565), 0.22 (R441), 0.55 (R362), and 0.39 (R495). The spectral sensitivities of *Arhopala* were investigated using the same techniques, as described briefly below. Computations were run on a MacPro running BBN RS/1 under WindowsXP.

Epi-Microspectrophotometry for Arhopala japonica

Following measurement of a dark-adapted eyeshine spectrum of *Arhopala japonica*, the eye was treated with Optics Technology interference filters, 633, 566, or 433 in separate experiments. This enabled measurement of difference spectra from partially bleached R570 (LW) and R440 (Blue) rhodopsins. Optophysiological spectral sensitivities were obtained by measuring pupillary responses using 30 sec flashes. For *A. japonica*, the eye was measured at Elevation 75° and Azimuth 35º creating a log10-sensitivity function well fit by rhodopsins R340 (UV), R436 (Blue), and R571 (LW). The absorbance spectrum for the second blue rhodopsin (R515) of *A. japonica* was computationally estimated using retinal densitometry analyses, as described for *E. atala*.

Eye anatomy

Eumaeus atala eyes were immersed for prefixation in 2.5% Glutaraldehyde/2% paraformaldehyde in 0.1M Sodium Cacodylate buffer (pH 7.4) (Electron Microscopy Sciences, PA, USA) for 2h at room temperature, then stored at 4°C for 12-14h. After washing with the same buffer solution at room temperature, the perfused fixed eye tissue was postfixed for 2h, washed in 0.1M Cacodylate buffer and postfixed in 1% Osmium tetroxide (OsO4)/1.5% Potassium ferrocyanide ($KFeCN_6$), washed in water and incubated in 1% uranyl acetate prior to successive alcohol dehydration steps. The tissue was then infiltrated in a 1:1 mixture of propylene oxide: embedding resin (TAAB Epon, Marivac Canada Inc. St. Laurent, Canada) for 48h at 4°C, prior to embedding in pure resin for polymerization at 60°C for 48h. A second resin polymerization step was performed following precise reorientation of the sample to 30° elevation in the dorsal region. Ultrathin 60 nm sections were cut on a Reichert Ultracut-S microtome equipped with a diamond blade and transferred to a formvar/carbon coated copper grid. To increase contrast prior to examination in the microscope, the grid was incubated for 3 min in 2% Uranyl acetate in 50% Acetone, rinsed in 50% Acetone, washed in water, and incubated in lead citrate for 30 s, blotting

the excess liquid off after each incubation using a Whatman filter paper. Grids were examined on a TecnaiG2 Spirit BioTWIN (or JEOL 1200EX) electron microscope equipped with a Hamamatsu ORCA HR camera (HV=80.0kV).

De novo Eumaeus atala eye transcriptome

The heads of 10 adult males (1 day old) were dissected under ambient light with their antennae, proboscis and palpi removed prior to flash freezing in liquid nitrogen. Total RNA was extracted using the Direct-zol RNA extraction kit (Zymoresearch, CA, USA). Illumina paired-end libraries were constructed using the Ultra II RNA Directional kit (New England Biolabs, USA) and sequenced with an Illumina HiSeq 2500. Adaptors were removed using Trimgalore (26) and low-quality reads were filtered out prior to generating a de novo assembly reference transcriptome for all libraries in the Trinity sequence assembly and analysis pipeline (27). This assembly resulted in 301656 transcripts with a contig N50 of 2519 bp, and average contig lengths of 1029 bp. Small fragments were filtered out based on expression values using Kallisto (28). Opsin sequences from two other lycaenids (5) were used as queries to identify all opsin mRNAs across tissues in the final assembly using BLAST (29). To confirm their identity, the candidate opsin sequences were blasted back to the NCBI non-redundant database.

LW opsin cDNA characterization

RNA was extracted from eye tissue preserved in RNA shield reagent (Zymo Research) for *A. japonica*. Samples were first removed from the storage solution with sterile forceps, briefly blot dried on a sterile Kimwipes paper, flash frozen in a mortar containing liquid nitrogen and finely ground using a cold pestle. Following RNA purification, we quantified RNA using a Quant-iT RNA kit and a Qubit fluorometer (Invitrogen). From purified RNA, we synthesized cDNA using the GoScript™ Reverse Transcription System (Promega) and amplified a central region of the long-wavelength opsin using oligonucleotide primers: 5'-TTGAAGCTTCARTTYCCNCCNATGAAYCC-3' (forward) and 5'-CGAATTCGTCATRTTNCCYTCIGGNACRTA-3' (reverse) (30). Single bands of expected sizes were obtained, and the PCR products were purified with Exo-SAP, following Sanger sequencing. We thereafter used the SMARTer RACE cDNA Amplification kit (Clontech) to prepare 5'- and 3'- RACE cDNA. We carried out RACE PCRs, and to increase the specificity of RACE reactions, we performed nested PCRs for each cDNA and obtained single-band PCR products, which were gel-purified using a Qiaquick Gel Extraction Kit (Qiagen), ligated into PCR2.1 (Invitrogen) and transformed into chemically competent TOPO10 cells (Invitrogen). Single bacterial clones were purified, and plasmid DNAs were sequenced using M13F and M13R primers at the Harvard DF/HCC DNA Resource Core. In total, we obtained sequences from 5 to 10 opsin clones for each RACE cDNA. Based on the 5'- and 3'-UTR information, gene-specific primers were designed and used in combination with respective eye cDNAs to confirm the integrity of each full-length LW opsin coding DNA sequence. Opsin subfamily phylogenetic placements were confirmed by aligning selected lepidopteran opsin genes extracted from Genbank using MAFFT as implemented in Geneious (31), and a Neighbor-Joining (NJ) tree of the aligned dataset was constructed using RAxML (32).

Functional assays

Small scale transfection and opsin expression optimization. HEKT293 cells were plated at a density of 0.6 x 10^6 cells in a 6-well culture dish containing DMEM medium (Gibco), and transfected after 48h (80% confluency) with a 1:3 ratio DNA (2 µg): PEI 1mg/mL (6 µL) (Polysciences, USA) diluted in Opti-MEM I Reduced Serum (Life Technologies). Transfected cells were harvested in cold D-PBS (Sigma-Aldrich) after 2 days, centrifuged at 4°C for 5 min at 4000 rpm, and resuspended in 50 µL Ripa lysis buffer (Invitrogen) supplemented with 1% n-Dodecyl β-D-maltoside (Sigma-Aldrich). Cell membranes were lysed for 1h at 4°C with gentle rotation on a sample homogenizer, and cell debris collected by centrifugation at 4°C for 15 min at 13,000 rpm. The crude protein lysate concentration was quantified by BSA (Sigma-Aldrich) and 25 µg crude extract was loaded on NuPAGE™ 3-8% Tris-Acetate gels (ThermoFisher) and transferred to a polyvinylidene difluoride membrane on a TurboBlotTransfer system (Biorad Laboratories). The membranes were blocked with 5% milk (Biorad) in tris-buffered saline containing 0.1% Tween 20 (TBS-T, Biorad) and incubated overnight with primary antibodies (aFLAG 1:2,500, aHSP90 1:50,000, GE Healthcare) containing 0.01% Sodium azide (Sigma Aldrich) on a gently rocking platform at 4°C. After washing with TBS-T the membranes incubated with aFLAG and aHSP90 were respectively incubated with HRP Conjugated ECL anti-mouse and ECL anti-rabbit (Amersham, USA), revealed using the SuperSignal West Femto (Thermo Scientific) and imaged on a ChemiDoc system (Biorad Laboratories). High-expressing clones from GPCR opsin cDNAs were transiently expressed in HEKT293 cells prior to large scale *in vitro* purification as described in the main text.

Opsin purification yields. Large-scale transfections typically produced 15-20 culture dishes yielding at least 120-150 x 10^6 cells at time of harvest. Following membrane solubilization, the crude protein extract was quantified by BSA according to the manufacturer's protocol (Thermo Fisher Scientific), and then compared with the total amount of opsin protein recovered in the eluate fraction (Table S7). On average, we quantified that the recombinant opsin proteins accounted for 216 µg /µL in 300 µL eluate, corresponding to 64.8 mg or 2.7% of the total cell protein content, although some recombinant opsins reached up to 5.5 %. This indicates that the presence of the C-terminal FLAG epitope

and 20 residue-long T2A peptide chain are compatible with proper folding of monomeric opsin proteins. We further calculated the $\lambda_{280}/\lambda_{max}$ ratio for each purification, and used this as an indicator of functional rhodopsin in the protein eluate (33), where λ_{280} corresponds to a combination of inactive opsins due to misfolding, mistrafficking or not forming an active rhodopsin with the chromophore in the membrane.

Spectral tuning mutagenesis

The EatBRh1 and EatBRh2 opsin amino acid sequences were uploaded to the SWISS-MODEL protein recognition engine (34) to generate a template aligned against the invertebrate squid rhodopsin crystal structure (PDB2Z73) (35). The predicted homology model for each blue opsin was analyzed in Pymol (36) to identify homologous binding sites in the 11-cis-retinal binding pocket within a range of 5Å from any carbon in the retinal polyene chain. Of the 101 amino acid substitutions that differ between the duplicate opsins, 21 residues were predicted to interact with the 11-cis-retinal chromophore, with 6 variant sites between both opsin sequences.

Amino acid sequences from blue opsins were retrieved from Genbank and aligned using the MAFFT package followed by NJ tree inference and support analysis derived from 1,500 bootstrap replicates in Geneious (31) prior to visualization in EvolView (37) with the squid rhodopsin as outgroup. The phylogeny was used to identify functionally convergent amino acid replacements repeatedly associated with similar shifts in absorption spectra between blue opsin duplicates. We identified amino acid positions that were likely to reside within the chromophore binding pocket of the opsin protein, and that also had diverging biochemical properties (charge and/or polarity). A BRh1 plasmid DNA construct was modified to incorporate 6 variant positions identified in BRh2, namely A116S, I120F, G175S, Y177F, I206C, and F207C.

Chimeric BRh1 rhodopsin constructs bearing single variant sites located on helix 3 (A116S, I120F), the β-strand located between helices 3 and 4 (G175S, Y177F), and on helix 5 (I205C, F206C) were purified and analyzed by spectroscopy in the native dark state. Since only A116S and Y177F had tuning effects in the range of interest, we combined coevolving adjacent site variants A116S/I120F, and G175S/Y177F and followed two distinct routes by successively adding variant sites creating triple mutants. Starting from a green-shifted BRh1 variant carrying I205C and F206C, a third trajectory was studied where variant sites A116S, I120F, Y177F were also successively added.

Supplementary References

1. W. C. Gordon, Microvillar Orientation in the Retina of the Nymphalid Butterfly. *Z. Naturforsch* **32**, 662-664 (1977).
2. G. Kolb, The structure of the eye of *Pieris brassicae* L. (Lepidoptera). *Zoomorphology* **87**, 123-146 (1977).
3. G. Kolb, Retinal ultrastructure in the dorsal rim and large dorsal area of the eye of *Aglais urticae* (Lepidoptera). *Zoomorphology* **106**, 244-246 (1986).
4. A. Palacios, T. Goldsmith, G. D. Bernard, Sensitivity of cones from a cyprinid fish (*Danio aequipinnatus*) to ultraviolet and visible light. *Vis Neurosci* **13**, 411-421 (1996).
5. M. P. Sison-Mangus, G. D. Bernard, J. Lampel, A. D. Briscoe, Beauty in the eye of the beholder: the two blue opsins of lycaenid butterflies and the opsin gene-driven evolution of sexually dimorphic eyes. *J Exp Biol* **209**, 3079-3090 (2006).
6. M. P. Sison-Mangus, A. D. Briscoe, G. Zaccardi, H. Knüttel, A. Kelber, The lycaenid butterfly *Polyommatus icarus*; uses a duplicated blue opsin to see green. *J Exp Biol***211**, 361 (2008).
7. G. Bernard, C. Remington, Color vision in *Lycaena* butterflies: spectral tuning of receptor arrays in relation to behavioral ecology. *Proc Nat Acad Sci USA* **88**, 2783-2787 (1991).
8. J. Stalleicken, T. Labhart, H. Mouritsen, Physiological characterization of the compound eye in monarch butterflies with focus on the dorsal rim area. *J Comp Physiol A Neuroethol Sens Neural Behav Physiol* **192** (2006).
9. F. D. Frentiu *et al.*, Adaptive evolution of color vision as seen through the eyes of butterflies. *Proc Nat Acad Sci USA* **104**, 8634-8640 (2007).
10. X. Qiu, K. Arikawa, The photoreceptor localization confirms the spectral heterogeneity of ommatidia in the male small white butterfly, Pieris rapae crucivora. *J Comp Physiol A* **189**, 81-88 (2003).
11. K. Arikawa, M. Wakakuwa, X. D. Qiu, M. Kurasawa, D. G. Stavenga, Sexual dimorphism of short-wavelength photoreceptors in the small white butterfly, *Pieris rapae crucivora*. *J Neurosci* **25**, 5935-5942 (2005).
12. A. Blake, P. Pirih, X. D. Qiu, K. Arikawa, Compound eyes of the small white butterfly *Pieris rapae* have three distinct classes of red photoreceptors. *J Comp Phys A* **205**, 553-565 (2019).
13. D. E. Nilsson, M. F. Land, J. Howard, Optics of the butterfly eye. *J Comp Phys A* **62**, 341-366 (1988).
14. N. Nagloo, M. Kinoshita, K. Arikawa, Spectral organization of the compound eye of a migrating nymphalid, the chestnut tiger butterfly *Parantica sita*. *J Exp Biol* **223**, jeb217703 (2020).
15. M. Wakakuwa *et al.*, Evolution and Mechanism of Spectral Tuning of Blue-Absorbing Visual Pigments in Butterflies. *PLOS ONE* **5**, e15015 (2010).
16. W. H. Miller, G. D. Bernard, Butterfly glow. *Journal of Ultrastructure Research* **24**, 286-294 (1968).
17. K. Arikawa, Spectral organization of the eye of a butterfly, *Papilio*. *J Comp Physiol* **189**, 791-800 (2003).
18. G. D. Bernard, D. G. Stavenga, Spectral sensitivities or retinular cells measured in intact, living flies by an optical method. *J Comp Physiol A* **134**, 95-107 (1979).
19. G. D. Bernard, Dark-Processes Following Photoconversion of Butterfly Rhodopsins. *Biophysics of Structure and Mechanism* **9**, 277-286 (1983).
20. A. Briscoe, G. D. Bernard, A. Szeto, L. Nagy, R. White, Not all butterfly eyes are created equal: Rhodopsin absorption spectra, molecular identification, and localization of ultraviolet-, blue-, and green-sensitive rhodopsin-encoding mRNAs in the retina of Vanessa cardui. *J Comp Neurol* **458**, 334-349 (2003).
21. T. Saito *et al.*, Spectral tuning mediated by helix III in butterfly long wavelength-sensitive visual opsins revealed by heterologous action spectroscopy. *Zoological Letters* **5**, 35 (2019).
22. A. Kelber, C. Thunell, K. Arikawa, Polarisation-dependent colour vision in *Papilio* butterflies. *Journal of Experimental Biology* **204**, 2469 (2001).

23. R. Wehner, G. D. Bernard, E. Geiger, Twisted and non-twisted rhabdoms and their significance for polarization detection in the bee. *J Comp Physiol* **104**, 225-245 (1975).
24. D. G. Stavenga, J. Numan, J. Tinbergen, J. Kuiper, Insect pupil mechanisms. II. Pigment migration in retinula cells of butterflies. *J Comp Phys A* **113**, 73-93 (1977).
25. G. D. Bernard, "Noninvasive optical techniques for probing insect photoreceptors" in Biomembranes Part H: Visual pigments and purple membranes I, Methods in Enzymology, P. L, Ed. (Academic Press, New York, 1982), vol. 81, pp. 752-759.
26. F. Krueger, "Trim galore." A wrapper tool around Cutadapt and FastQC to consistently apply quality and adapter trimming to FastQ files. **516**, 517 (2015).
27. B. J. Haas *et al.*, De novo transcript sequence reconstruction from RNA-seq using the Trinity platform for reference generation and analysis. *Nat Prot* **8**, 1494-1512 (2013).
28. N. Bray, H. Pimentel, P. Melsted, L. Pachter, Near-optimal probabilistic RNA-seq quantification. *Nature Biotechnology* **34**, 525-527 (2016).
29. S. F. Altschul *et al.*, Gapped BLAST and PSI-BLAST: a new generation of protein database search programs. *Nucleic Acids Research* **25**, 3389-3402 (1997).
30. M. Wakakuwa, D. G. Stavenga, M. Kurasawa, K. Arikawa, A unique visual pigment expressed in green, red and deep-red receptors in the eye of the small white butterfly, *Pieris rapae crucivora*. *J Exp Biol* **207**, 2803-2810 (2004).
31. M. Kearse *et al.*, Geneious Basic: An integrated and extendable desktop software platform for the organization and analysis of sequence data. *Bioinformatics* **28**, 1647-1649 (2012).
32. A. Stamatakis, RAxML version 8: a tool for phylogenetic analysis and post-analysis of large phylogenies. *Bioinformatics* **30**, 1312-1313 (2014).
33. J. Morrow, B. Chang, The p1D4-hrGFP II expression vector: A tool for expressing and purifying visual pigments and other G protein-coupled receptors. *Plasmid* **64**, 162-169 (2010).
34. A. Waterhouse *et al.*, SWISS-MODEL: homology modelling of protein structures and complexes. *Nucleic acids research* **46**, W296-W303 (2018).
35. M. Murakami, T. Kouyama, Crystal structure of squid rhodopsin. *Nature* **453**, 363 (2008).
36. The PyMOL Molecular Graphics System, Version 1.8, Schrödinger, LLC.
37. H. Zhang, S. Gao, M. Lercher, S. Hu, W.-H. Chen, EvolView, an online tool for visualizing, annotating and managing phylogenetic trees. *Nucleic Acids Res* **40**, W569-W572 (2012).

Supplementary Figures

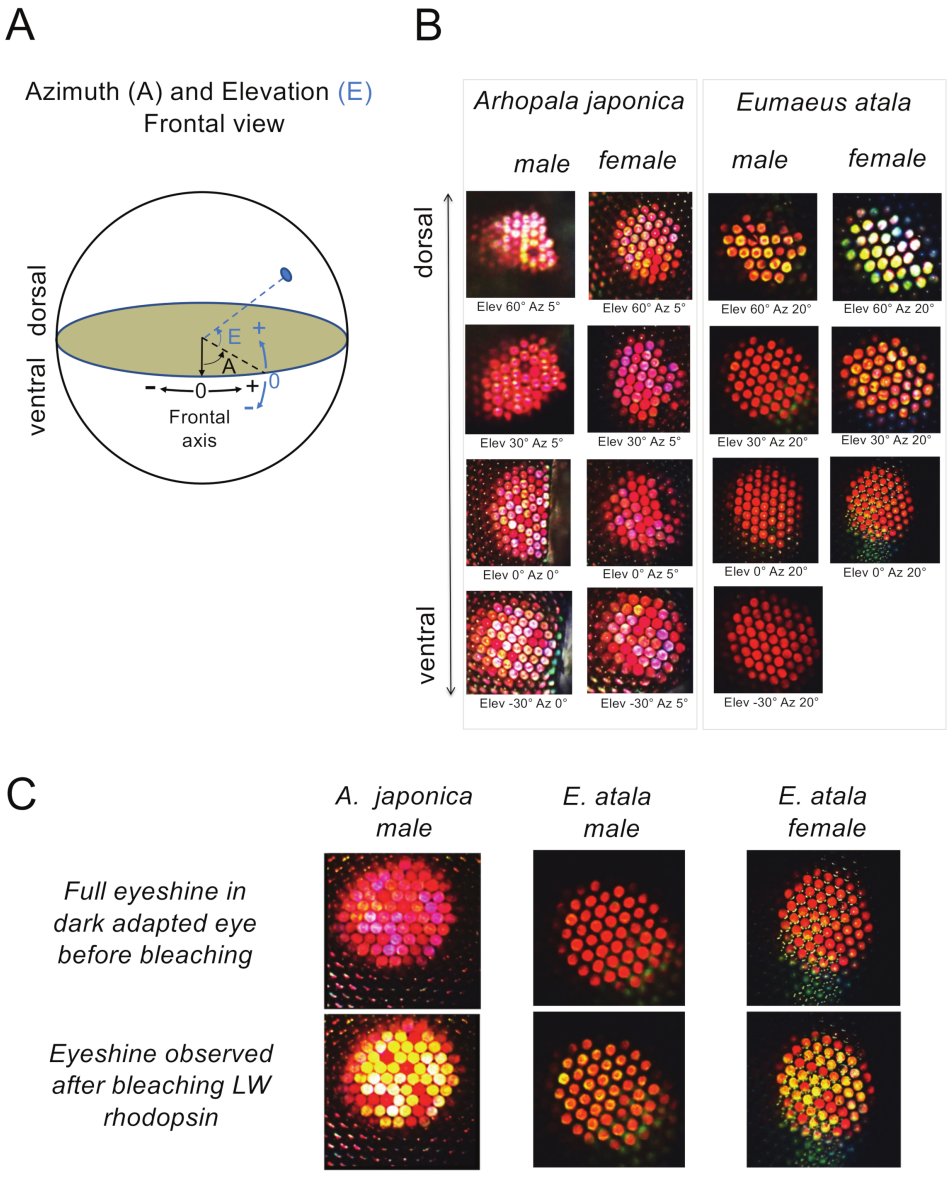

Fig. S1. Eyeshine from surveyed lycaenid butterfly compound eyes. Eyeshine patterns were obtained from 21º eye patches, at various elevation angles in *Arhopala japonica* and *Eumaeus atala*. (*A*) Schematic representation of Azimuth and Elevation angles. (*B*) Epi-illumination of dark-adapted eyes shows light reflected from patches of ommatidia viewing the incident illumination from dorsal to ventral elevations. Eyeshine varies between species and also to some extent along the dorso-equatorial gradient of a single eye. In *A. japonica* and *E. atala*, the ommatidia appear saturated in red eyeshine, indicating the presence of red-sensitive photoreceptor cells, some of which contain filtering pigment granules located distally within the photoreceptor cells. *(C)* Change in eyeshine patterns caused by bleaching of LW rhodopsin with 1 sec white-light flashes separated by 1 min dark periods, in *A. japonica* and *E. atala*. Lateral filtering pigments are not light sensitive and, whereas all rhabdomeres are filled with the LW rhodopsin, only those surrounded by cherry-red pigments remain red after bleaching the LW rhodopsin.

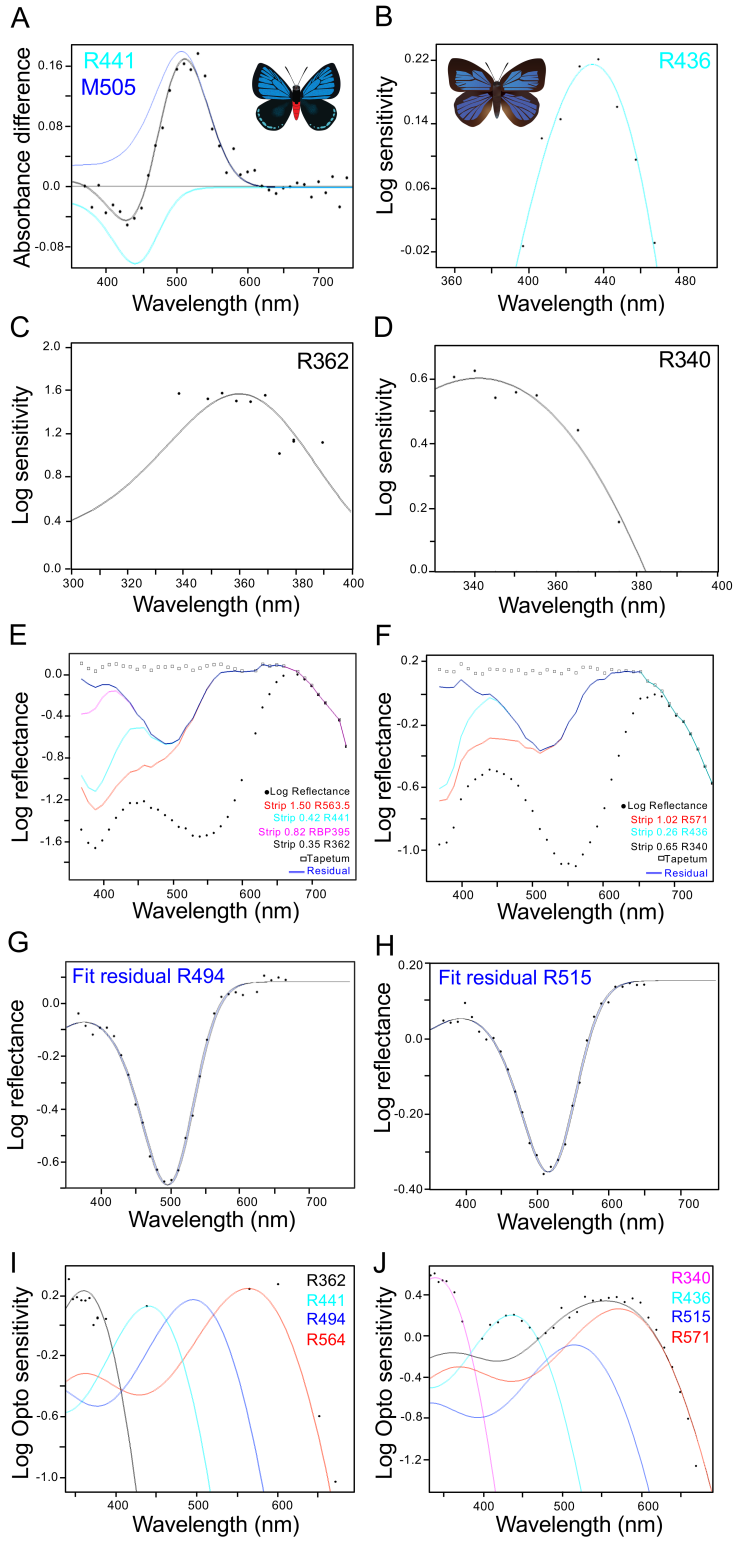

Fig. S2. *In vivo* evidence for shifted blue and red rhodopsins in lycaenid butterflies.
(*A*) Photochemical analysis of an *Eumaeus atala* eyeshine using an epi-microspectrophotometer. Log-reflectance difference absorbance spectra (DS, filled circles) and fitted curves (solid line) measured from dark-adapted eyes via partial-bleaching experiments of R441. M505, metarhodopsin. (*B-D*) Optophysiological analyses in *Arhopala japonica* and *E. atala* designed to measure pupillary sensitivity in the blue and ultraviolet range, to identify R436 in *A. japonica* (*B*), and UV rhodopsins with λ_{max} at 362 nm for *E. atala* (*C*) and 340 nm for *A. japonica* (*D*). (*E-F*) Densitometric analysis of an epi-microspectrophotometric reflectance spectrum of an *E. atala* eye (*E*) and an *A. japonica* eye (*F*). Completely dark-adapted eyeshine is used to confirm the contribution of each estimated visual pigment in the eye. The black dots plot the log-reflectance spectrum. The red curves are the spectra after having computationally stripped optical density (OD) of the LW rhodopsin such that the residual spectrum is flat from 565-570 nm to 660 nm. The cyan curves are the log-reflectance spectra after having stripped R441 (*E*) or R436 (*F*) to produce a residual flat from 450 nm. The blue curve is the log-reflectance spectrum after stripping RBP395 and R360 (*E*) or R340 (*F*), leaving a residual spectrum (double blue line) fit by a fourth rhodopsin at R494 in *E. atala* (*G*) and R515 in *A. japonica* (*H*). Stripping the R495 or R515 residuals leaves the curve plotted in open squares in (*E*) and (*F*), respectively, that is the putative average log-reflectance spectrum of the tapetum, that is flat from the UV out to 660 nm. (*G-H*) Computational analysis of the residual reflectance spectra supports the contribution of a fourth opsin pigment with λ_{max} peaking around 494 nm and 515 nm. (*I-J*) Optophysiological spectral sensitivity. Sensitivity data from an optophysiological threshold experiment measured at wavelengths close to *in vivo* λ_{max} values of the four rhodopsins in *E. atala* (*I*) and *A. japonica* (*J*). This shows that sensitivities at 441 nm and 494 nm cannot possibly be driven by R564 in *E. atala*. Likewise, sensitivities at 436 nm and 515 nm are not driven by R571 in *A. japonica*. Black dots are optophysiological log10-sensitivity data, each point being the reciprocal of the quantum flux that actually produced the criterion pupillary response at each measured wavelength. Curves in black or magenta, ultraviolet rhodopsin; curve in cyan, blue rhodopsin 1; curve in blue, blue rhodopsin 2; curve in red, long-wavelength rhodopsin. Long-wavelength sensitivity thus extends towards the far red due to both a novel type of red-shifted rhodopsin receptor and a green-shifted blue duplicate rhodopsin. Butterfly illustrations: JML.

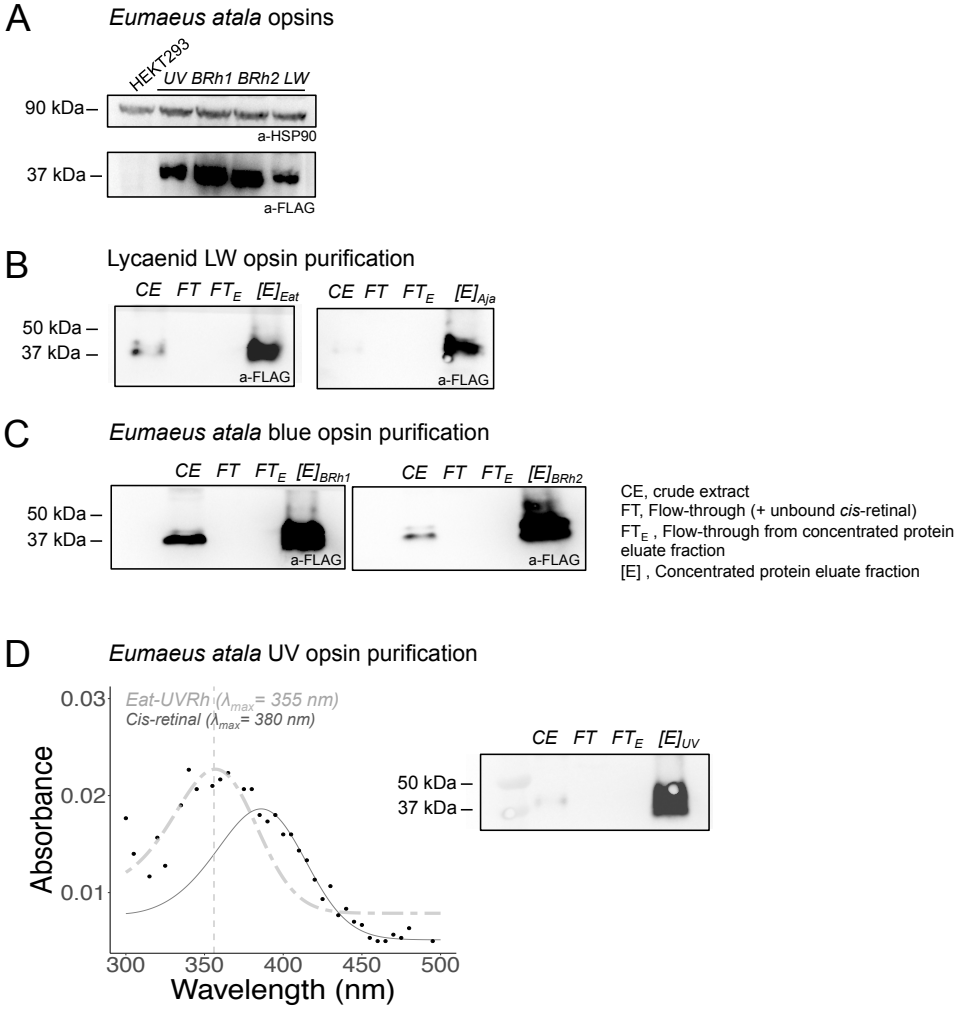

Fig. S3. Western Blot analyses of purified rhodopsins reconstituted in HEK293T cells. (*A)* Total membrane protein lysates of UV, Blue and LW opsins in *E. atala* following expression in the pCDNA-FLAG-T2A-Mruby2 expression cassette. HEKT293 cells were seeded at a density of $0.6.10^6$ cells in 6-well plates in DMEM medium containing 10% FBS and transfected the next day with pcDNA plasmids bearing opsin-FLAG-T2A-mRuby constructs. Transfection medium was replaced with fresh medium after 6 hours in all wells. Cells were cultured for 48 hours alongside untransfected control cells. Cells were washed and harvested in cold D-PBS buffer and centrifuged for 4 min at 4,000 rpm at 4°C. The cell pellet was resuspended in Ripa extraction buffer (Invitrogen) supplemented with 1% n-dodecyl -D-maltoside (DDM) (Sigma-Aldrich) and incubated for 1 hour at 4°C, on a gently rotating platform. Debris were centrifuged at 4°C for 15 min at 14,000 rpm and the crude extract supernatant was placed on dry ice. An aliquot was subsequently used for BSA analysis. Each lane contains 20 ug total protein extract diluted in 4x Laemmli buffer (Biorad) and containing 1% β-mercaptoethanol (Sigma). Samples are separated on NuPAGE 3-8% Tris-Acetate gradient gels (ThermoFisher Scientific) under non-denaturing conditions for 3 hours at 4°C and 80 Volts. After transfer to nitrocellulose membranes, low size and high size blotted bands were processed in parallel with primary antibodies anti-FLAG (1:1,000, GE Healthcare) or anti-Hsp90 (1:50,000; GE Healthcare), respectively, then with corresponding secondary antibodies ECL anti-mouse IgG (1:10,000, GE Healthcare) or polyclonal ECL anti-rabbit IgG (1:10,000; GE Healthcare), respectively. Lane 1: MW marker, lane 2: Supernatant of control untransfected cells, lanes 3-6: supernatant of cells transfected with *E. atala* UVRh opsin (44.34 kda), BRh1 opsin (43.18 kda), BRh2 opsin (43.07 kda) and LWRh opsin (41.9 kda). The expected molecular weight of monomeric units is indicated in parentheses. (*B)* Western blot analysis of *E. atala* LW rhodopsin purification and (*C)* EatBRh1 and EatBRh2 purification. HEKT293 cells were transfected with high-expressing opsin-FLAG-T2A-mRuby clones validated in a 6-well plate expression procedure. Transfected cells expressing rhodopsin were cultured in the dark in the presence of cis-retinal and harvested after 48hr as described in the methods. Cell membranes were solubilized, and the opsin-FLAG proteins were separated from the protein crude extract using 3x-FLAG-resin column purification prior to competitive binding with FLAG-peptide. The rhodopsin complexes were eluted and concentrated in 10-kda Amicon-columns. CE, crude extract; FT, Column flow through; $(FT)_E$, flow through from 10-kda concentration column retaining opsin-FLAG proteins; (E), Concentrated eluate fractions. Expected molecular weight: *Arhopala japonica* LWRh 41.97 kda. (*D)* Dark spectra of *Eumaeus atala* ultraviolet rhodopsin (UVRh) expressed using the HEK293T transient cell culture system.

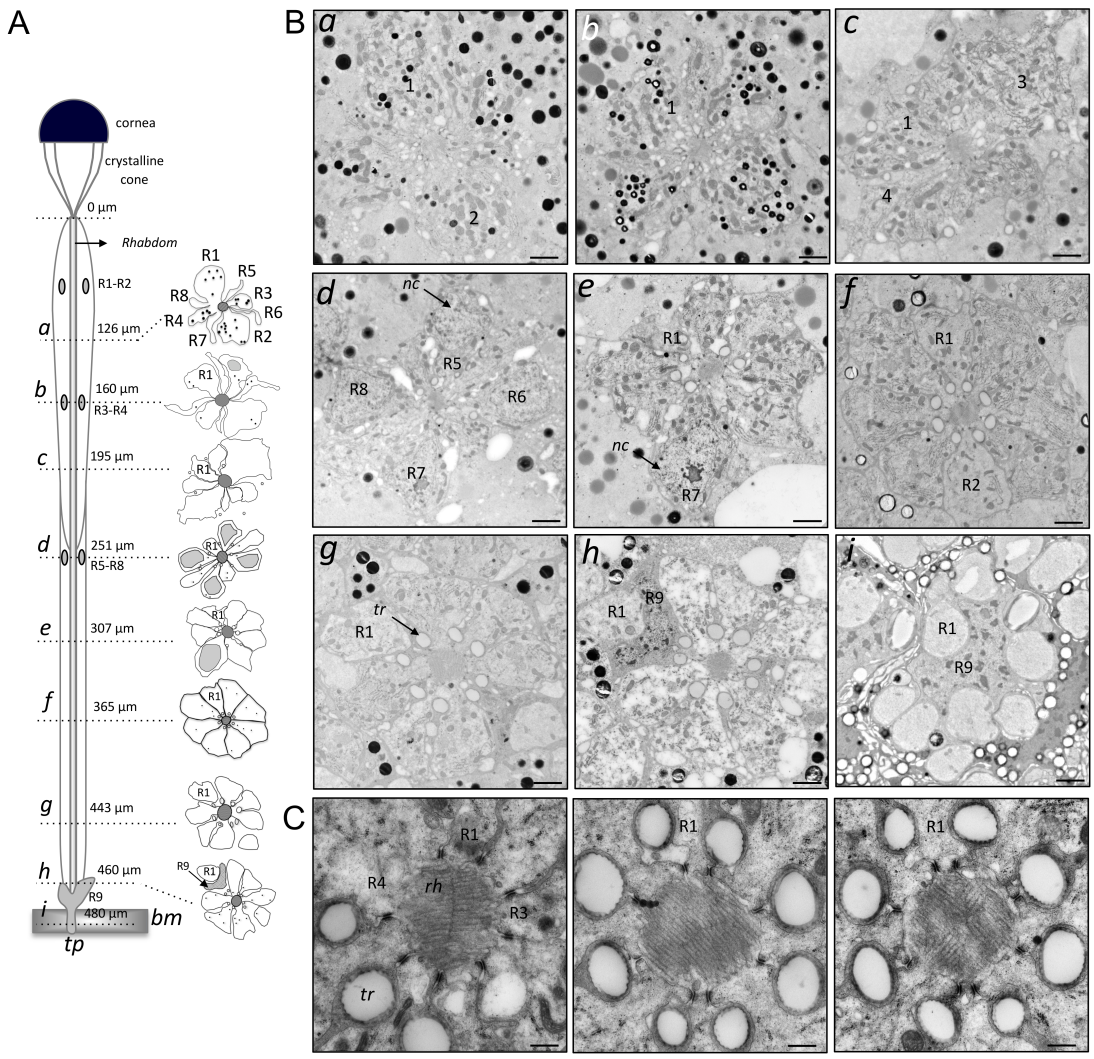

Fig. S4. Anatomical roadmap of a typical ommatidium in *Eumaeus atala*. (*A*) Diagram illustrating a typical ommatidium and the relative contributions of eight photoreceptor cells (R1-R8) and a ninth basal cell (R9) along the 480-µm long rhabdom. Photoreceptors R1 and R2 are distal cells in region *a* (126 µm) that contribute vertical microvillar structures containing UVRh, BRh1, and BRh2 rhodopsins. Photoreceptors R3-R4 and R5-R8 are distal and proximal cells, respectively, containing the LWRh rhodopsin (see Fig. 3). The basal cell, R9 is restricted to the region close to the basement membrane (460 µm, *h*). Although no microvillar projections were observed here, this basal cell has been found to contribute a few microvilli in other butterfly species (1-3). The mRNA opsin type expressed in this cell was not investigated. (*B*) Transmission electron micrographs (TEM) from a male dorsal eye region at 30° elevation across the rhabdom corresponding to rhabdomeric regions *a-i* as illustrated in (*A*). Scale bars, 2 µm. (*C*) Rhabdom ultrastructure of the ommatidia in the proximal retina. As described in detail in some butterflies (1, 14), the microvilli in the mid and proximal retina slowly develop alternating degree segments, here shown in regions *e* and *f,* where R1-R2 have become axonal and R3-R8 cell microvilli expand and dominate the rhabdom. At 307 µm, R3-R4 contribute long straight microvilli which are distally horizontal, and orthogonal to R1-R2. With increasing microvilli contributions from diagonal proximal receptors R5 to R8 (middle and right panels, 365 µm), additional rhabdom directions are observed. The rhabdomere axis in adjacent ommatidia can develop 45 and 135 diagonal microvilli (middle panel) or interdigitated (right panel) patterns. The microvillar twist along the distal-proximal rhabdom is thought to reduce self-screening to maintain spectral sensitivity narrow in long rhabdoms and reduce polarization sensitivity to help stabilize color vision (22, 23). Scale bars, 500 nm. *bm,* basement membrane*; rh,* rhabdom*; nc,* nucleus*; tr*, tracheole; *tp,* tapetum; 1-9, photoreceptor cells R1 to R9.

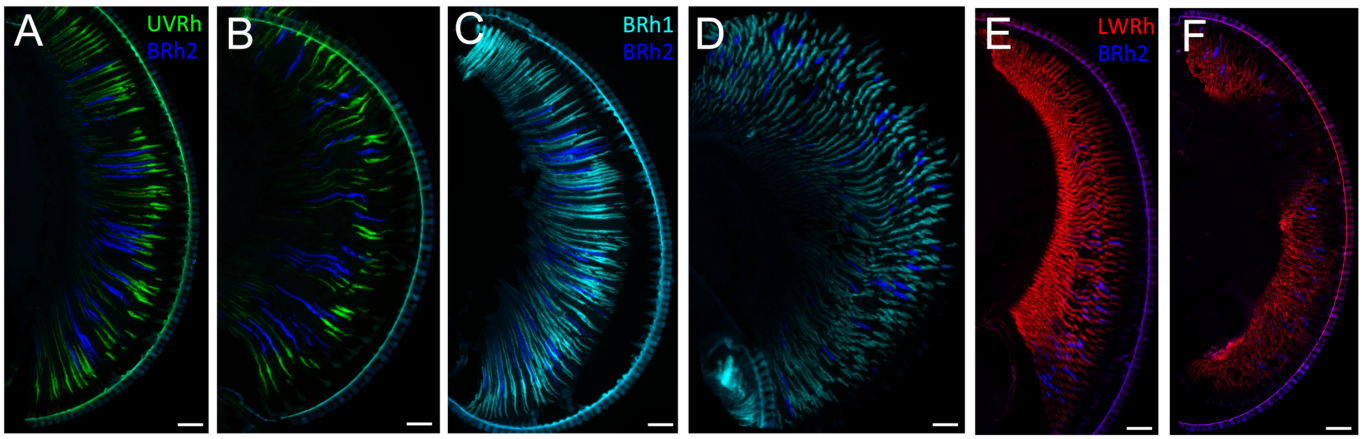

Fig. S5. Dorso-ventral opsin expression patterns. of BRh2 opsin mRNA in *Eumaeus atala*. Double fluorescent *in situ* hybridization for combinations of cRNA probes hybridizing to UVRh-BRh2 mRNAs in females (*A*) and males (*B*), BRh1-BRh2 mRNAs in females (*C)* and males (*D*), LWRh-BRh2 mRNAs in females (*E)* and males (*F*). BRh2 is more abundant in equatorial and ventral female ommatidia than in upper dorsal ommatidia (*A,C,E)* and is expressed dorsoventrally in males (*B,D,F).* Section orientation: Dorsal (top) to ventral (bottom). Scale bars, 100 µm.

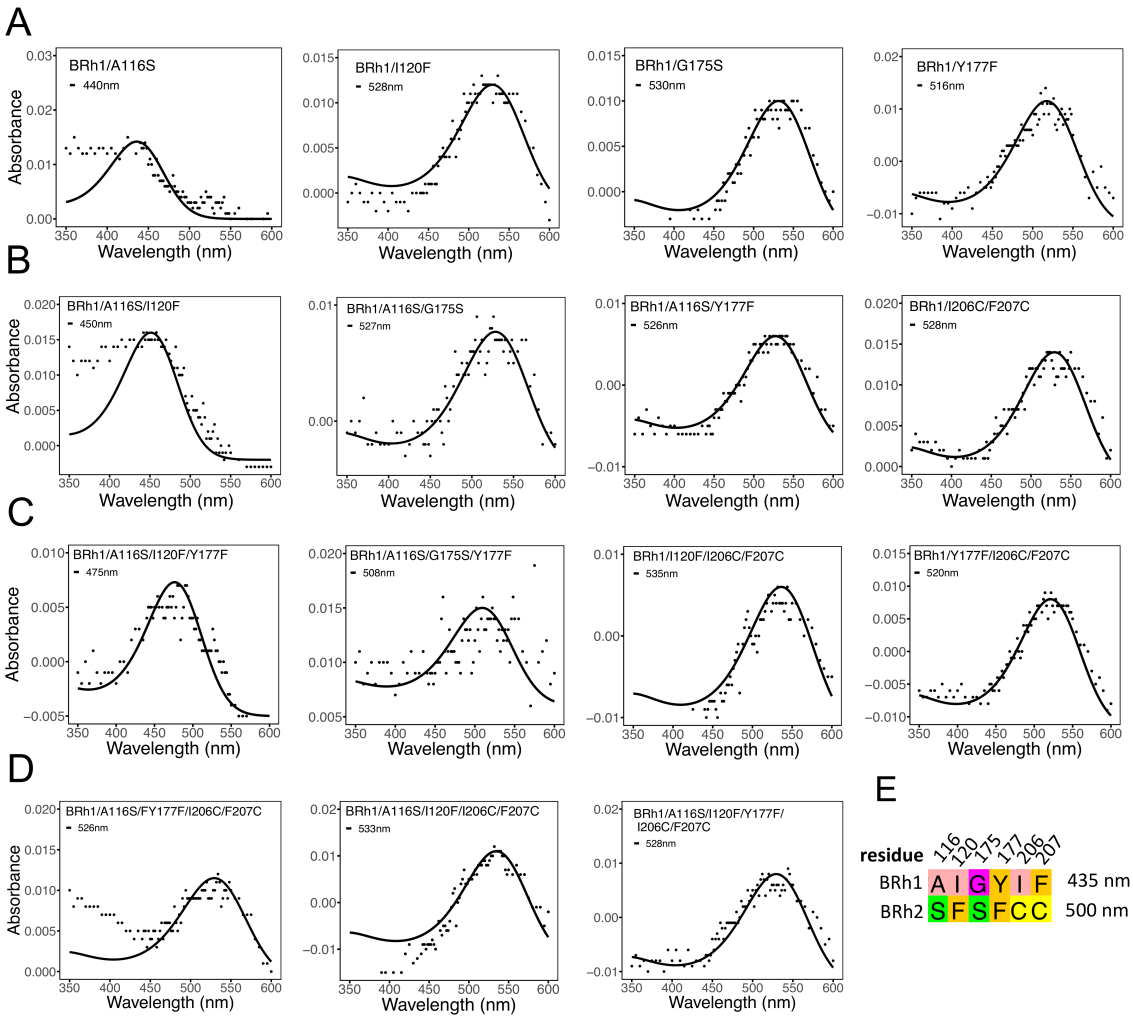

Fig. S6. Spectral tuning effect of EatBRh1 rhodopsin variants. Chimeric EatBRh1 rhodopsin plasmid constructs bearing EatBRh2 nucleotide substitutions were obtained via PCR-targeted mutagenesis, expressed transiently in cell cultures and purified *in vitro*. Each graph represents the absorbance values for an EatBRh1 variant rhodopsin (black dots) and the black lines represent the least-squares fitted Bernard rhodopsin template function at maximum absorption (λ_{max}). (*A)* Single-residue variants. (*B)* Two-residue variants. (*C)* Three-residue variants. (*D)* Four and five-residue variants. (*E)* Schematic view of mutated residues between blue opsin EatBRh1 (λ_{max} = 435 nm) and green-shifted blue opsin EatBRh2 (λ_{max} = 500 nm).

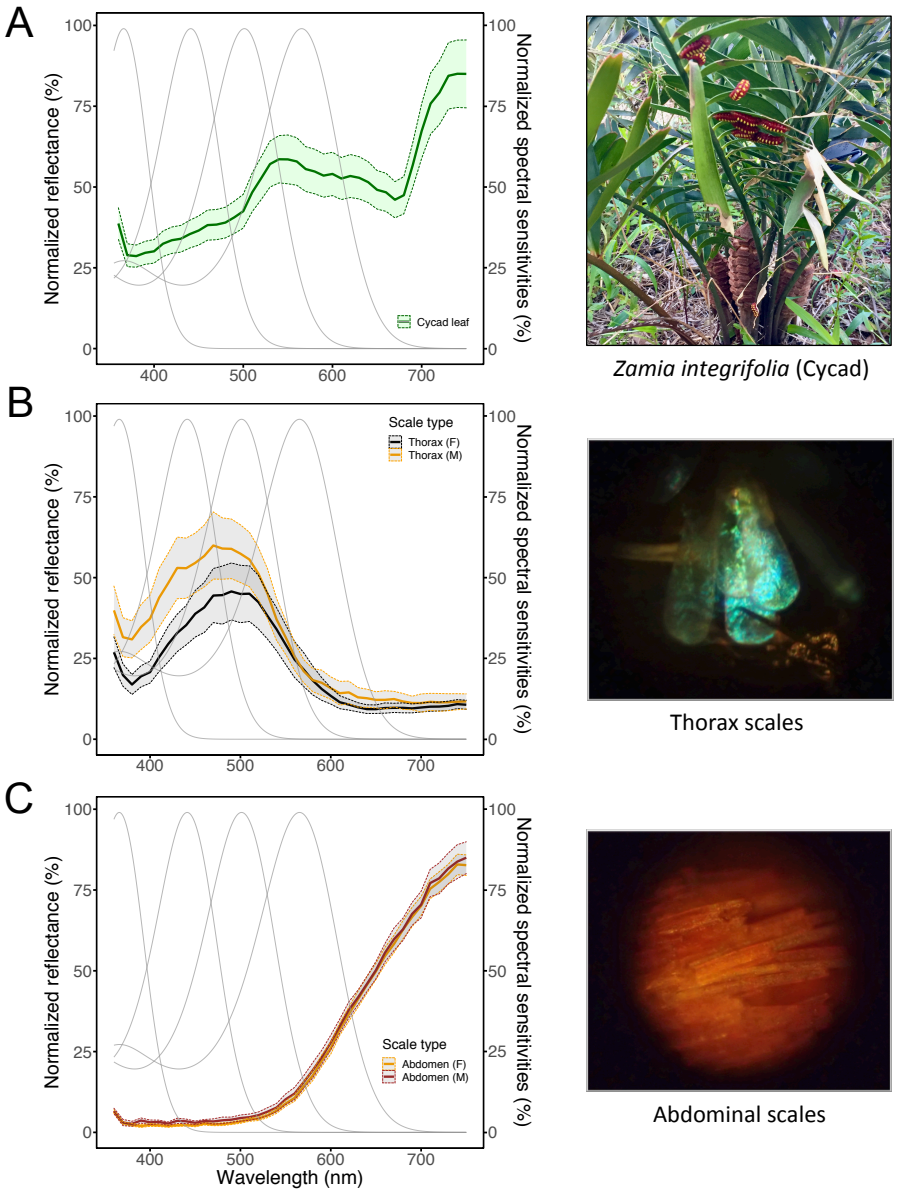

Fig. S7. Normalized reflectance spectra of cycad leaf and body scale coloration. (*A*) Cycad host plant (*Zamia integrifolia*) leaf reflectance spectra ± standard errors of the mean (N leaf measurements = 4). Right, *E. atala* larvae feeding on cycad leaves. Scale bar = 1 cm. (*B*) Thorax scale reflectance spectra ± standard errors of the mean (Measurements, 5-8), and photograph (right). (*C*) Abdominal scale reflectance spectra and photograph (right). The photographs in (*B, C*) are magnified views of representative scales in patches measured by epi-microspectrophotometry (MSP). The field of view for each photograph is 210 µm in diameter. Grey curves represent the normalized rhodopsin spectral sensitivities in *Eumaeus atala*. F, female; M, male. Photograph credits: *A*, NEP; *B*-*C*, GDB.

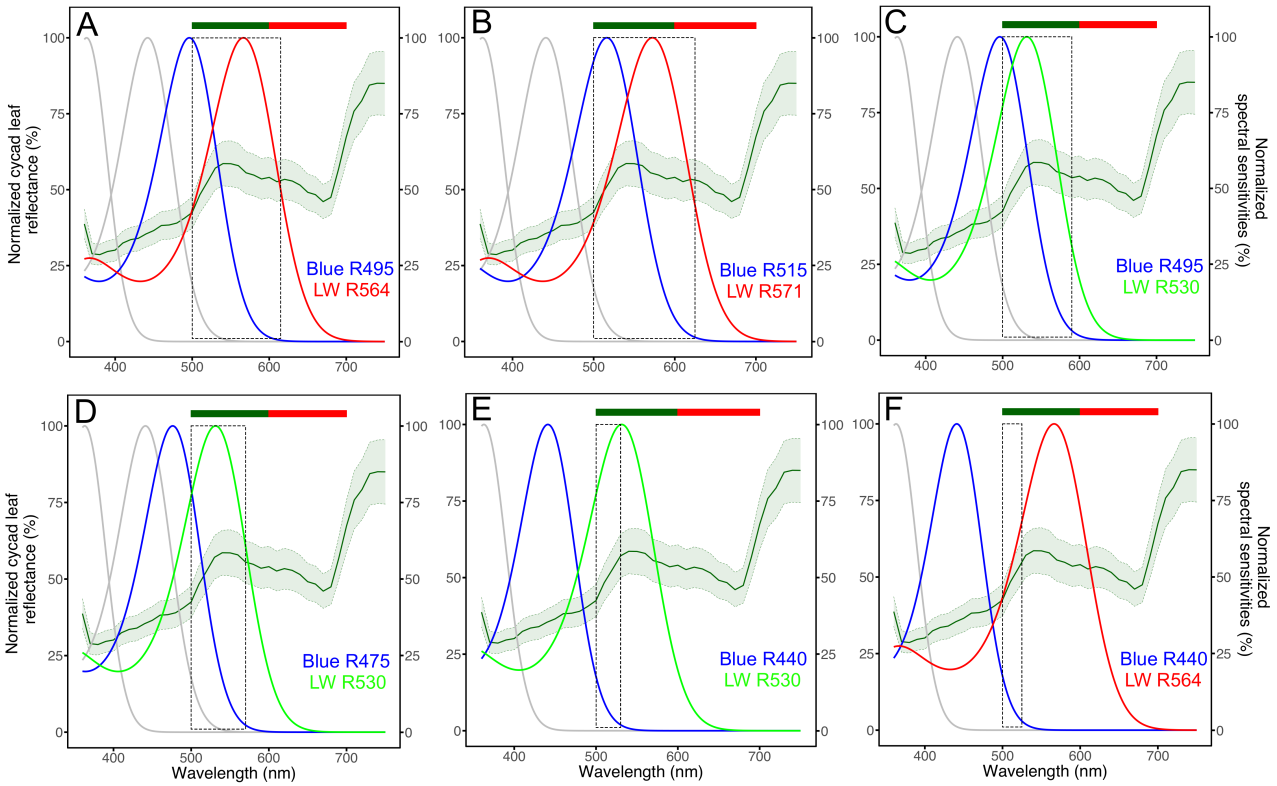

Fig. S8. Color discriminability analysis at long wavelengths against leaf reflectance spectra using visual systems with distinct photoreceptor sensitivities. (*A-F*) The dark green curves represent the cycad leaf reflectance normalized to 550 nm (from Fig. S7). The dark green line represents the mean leaf reflectance. Shaded green areas correspond to the standard errors of the mean. The green and red rectangles represent the wavelength range for green (500-600 nm) and red (600-700nm) colors, respectively. Solid grey lines indicate normalized UV (R362) and blue (R440) (*A-D*) or UV (*E-F*) photoreceptor spectral sensitivity of the *E. atala* eye. Dotted black rectangles indicate the wavelength range for color discriminability using Blue and LW opsins with variable spectral sensitivities. (*A*) Color discriminability potential of *E. atala*. Solid blue lines indicate the Blue-shifted (R495) photoreceptor spectral sensitivity of the second blue opsin in *E. atala*. The solid red line corresponds to the long-wavelength spectral sensitivity (R564). With a 5% sensitivity threshold, *E. atala* is expected to be able to discriminate colors at long wavelengths in the range 500-615 nm (dotted black rectangle). (*B*) Color discriminability in the range 500-625 nm (dotted black rectangle) for a visual system using R515 and R571, similarly to *A. japonica*. (*C*) Color discriminability would extend from 500 to 590nm for a visual system with a green-shifted blue opsin and a green long-wavelength opsin. (*D-E*) Intermediate blue spectral sensitivities (*D*, R475; *E*, R440) are expected to reduce color vision in the green range to 500-570nm (*D*) and 500-550 nm (*E*). (*F*) A visual system with a single R440 blue opsin and a red-shifted LW opsin is expected to confer the most limited color discrimination range (500-525nm). This indicates that visual systems with correlated opsin tuning such as *E. atala* and *A. japonica* are likely to extend color discrimination at long wavelengths.

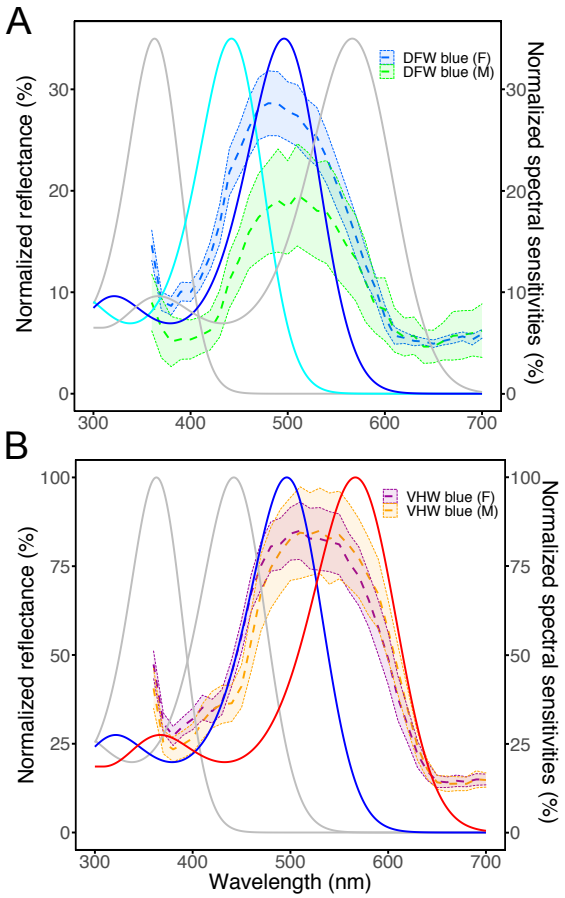

Fig. S9. Wavelength discriminability of *E. atala* wing coloration. (*A*) Overlap between R440 (cyan solid curve) and R495 (blue solid curve) and reflectance spectra from dorsal forewing (DFW) blue pigmentation of males (M) and females (F). Grey curves indicate R362 and R565. (*B*) Overlap between R495 (blue curve) and R565 (red curve) and reflectance spectra from ventral hindwing (VHW) blue pigmentation of males and females. Grey curves in (*B*) indicate R362 and R440. See also Fig. 5.

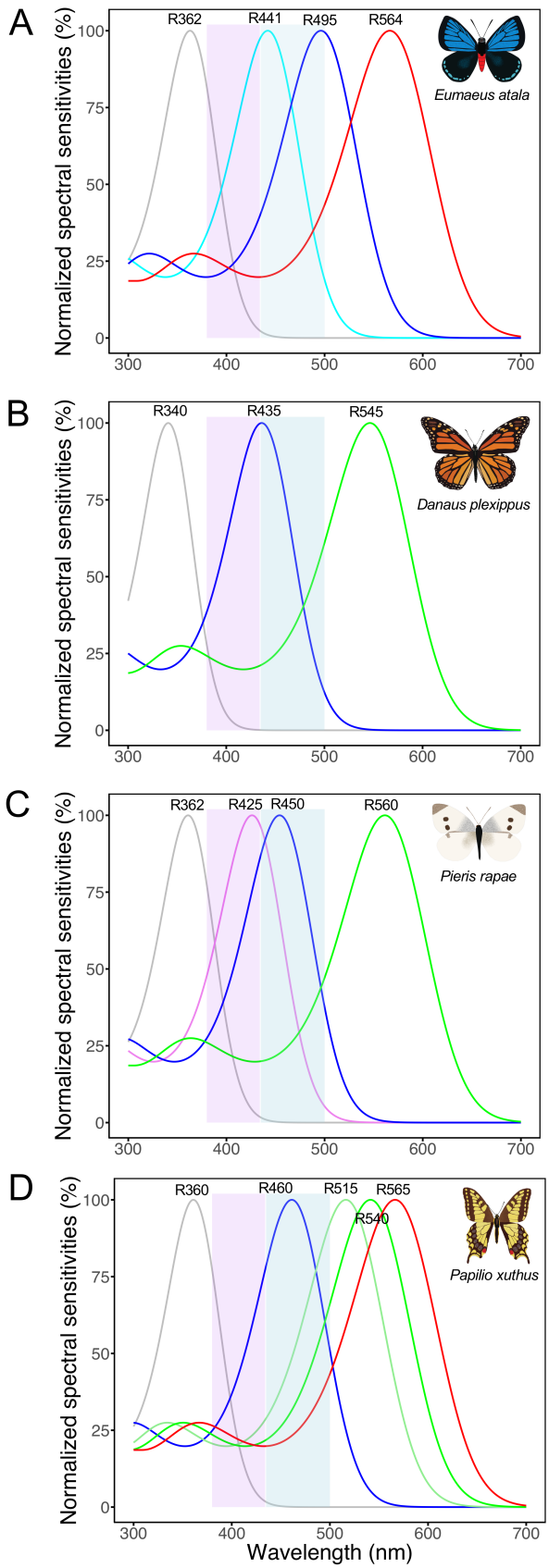

Fig. S10. Spectral richness and wavelength discrimination in the violet and blue range across model butterfly visual systems. (*A-D*) Normalized absorbance spectra of butterfly rhodopsin sensitivities using the Bernard template (4). The purple and blue rectangles represent the wavelength range for violet light (380-435nm) and blue light (435-500nm). (*A*) The eye of the lycaenid *Eumaeus atala* contains four rhodopsins (R) with λ_{max} values corresponding to R362, R440, R495, R564 (see also Fig. 2, Fig. S2, Fig 4), similarly to values estimated by microspectrophotometric measurements for the eyes of *Lycaena rubidus* and *Polyommatus icarus* (5-7). (*B*) The eye of *Danaus plexippus* contains three rhodopsins with λ_{max} values of R340, R435 and R545 estimated from microspectrophotometric measurements (8, 9). (*C*) The eyes of the pierid *Pieris rapae* express four rhodopsins with λ_{max} values estimated from intracellular recordings at R360, R425, R450 and R563 (10-12), and with R425 and R450 absorbance spectra further confirmed via heterologous expression (15). (*D*) The eye of the papilionid *Papilio xuthus* contains five rhodopsins, R360, R460, R515, R540, R565 estimated via intracellular recordings (17) and spectroscopy (21). The additional classes of red receptors conferred by lateral filtering of the LW opsin in *Pieris* and *Papilio* are not represented here. Butterfly illustrations: JML.